Impact of Atmospheric Forcing Data Quality on Numerical Prediction of Coupled Atmosphere–Ocean Dynamics: Tropical Cyclone Asna in the Northern Indian Ocean

Mahyar Majidy Nik[1], Amir Ashtari Larki [2*]

[1] Ph.D. Student in Physical Oceanography, Department of Physical Oceanography, Faculty of Marine Science and Oceanography, Khorramshahr University of Marine Science and Technology, Khorramshahr, Iran
[2] Department of Physical Oceanography, Faculty of Marine Science and Oceanography, Khorramshahr University of Marine Science and Technology, Khorramshahr, Iran*

ARTICLE INFO

Article History:
Received….
Accepted ….
Available online ….

Keywords:
Ocean-Atmospheric Modeling
Coupled Model
Tropical Storm
Sea State Forecasting

ABSTRACT

Accurate prediction of atmosphere–ocean conditions in coastal and offshore regions requires high-quality input data and reliable coupled atmosphere–ocean modeling. In this study, two datasets—GFS forecast data and GFS reanalysis data—were employed to evaluate the performance of atmospheric and wave models in reconstructing the conditions of Tropical Cyclone Asna (2024) over the northern Indian Ocean. The results showed that limitations in the quality of GFS forecast data led to an inadequate representation of the intensity and structure of surface winds, and this weakness was directly reflected in the WWIII wave model. Consequently, the simulated significant wave height (SWH) was underestimated compared with observational or reanalysis values, and the timing of the wave peaks exhibited delays and unrealistic fluctuations. In contrast, the GFS reanalysis data successfully reproduced the wave growth and decay processes as well as the spatiotemporal structure of the storm with higher accuracy. However, due to their retrospective nature, these data are not applicable for operational real-time forecasting.
These findings clearly indicate that the lack of high-quality and up-to-date atmospheric input data is the main obstacle to producing accurate atmosphere–ocean forecasts in the target regions, and that relying solely on global operational datasets such as forecast or reanalysis cannot fully capture the dynamic and thermodynamic characteristics of tropical cyclones. Accordingly, the necessity of developing and implementing a native coupled atmosphere–ocean model at both global and regional scales is evident. Such a model, by integrating local observational data and advanced data assimilation techniques, can provide more accurate initial and boundary conditions and enable the production of forecasts with higher accuracy and reliability. Achieving this capability will be a fundamental step toward strengthening scientific and operational capacity in physical oceanography and will pave the way for applying modeling results to secondary marine and coastal activities such as crisis management, maritime safety, coastal infrastructure design, and the sustainable exploitation of marine resources.

1. Introduction

The Indian Ocean, the third-largest oceanic basin on Earth, encompasses approximately 20% of the planet's surface area, ranking after the Pacific and Atlantic Oceans. Deriving its name from the Indian subcontinent, it is regarded as the geologically youngest of the major oceans. Geographically, the Indian Ocean is bounded to the north by the southern margins of the Arabian Sea and the Laccadive Sea; to the west by the Arabian Peninsula and the African continent; to the east by the Malay Peninsula, the Sunda Archipelago, and Australia; and to the south by the Southern Ocean. Its boundary with the Atlantic Ocean is conventionally defined by the 20°E meridian extending southward from Cape Agulhas, while its separation from the Pacific Ocean is delineated by the 146°49′E meridian extending southward from the southernmost tip of Tasmania. The northernmost reach of the Indian Ocean lies at approximately 30°N latitude within the Persian Gulf [7].
The Indian Ocean encompasses an estimated area of 70,560,000 km², inclusive of the Red Sea and the Persian Gulf, with a total volume approximated at 292,131,000 km³. It is bordered by four continents—

Asia, Africa, Antarctica, and Australia—thereby occupying a central position in the global oceanic system. The basin contains approximately 1,382 islands, among which Madagascar, Sri Lanka, Nias, and Socotra represent the largest and most prominent landmasses.

The Indian Ocean extends approximately 9,600 km from Antarctica to the Bay of Bengal and spans about 7,600 km between Western Australia and the Eastern coast of Africa. Its mean depth is estimated at 3,890 m (12,762 ft). Major marginal seas associated with the Indian Ocean include the Mozambique Channel, the Red Sea, the Persian Gulf, the Andaman Sea, the Arabian Sea, and the Bay of Bengal, among others [4].

In addition, the Indian Ocean encompasses four strategically significant maritime chokepoints that are critical for international trade: the Suez Canal in Egypt, the Bab al-Mandeb Strait (between Djibouti and Yemen), the Strait of Hormuz (between Iran and Oman), and the Strait of Malacca (between Indonesia and Malaysia). These waterways constitute essential corridors for the global energy trade, a resource of both strategic and economic importance, and collectively function as a major conduit for the international supply of energy. The northern Indian Ocean, in particular, represents the most critical energy transportation route, as it links the hydrocarbon-rich states of West Asia to global markets. On average, more than 17 million barrels of crude oil are transported daily from the Persian Gulf through this region, while over 40% of the world's offshore oil production originates from the Indian Ocean, primarily from the petroleum fields of Indonesia and the Persian Gulf [13].

Beyond their geopolitical significance, wind and wave regimes in the Indian Ocean exert a critical influence on the design, operation, and resilience of marine infrastructure. The hydrodynamic characteristics of this basin—particularly under extreme conditions generated by tropical cyclones and monsoonal storms—directly affect the structural integrity and operational safety of ports, offshore oil platforms, submarine pipelines, and coastal defense systems. Moreover, wind-generated waves play a fundamental role in governing coastal and oceanic processes, including water circulation, sediment transport, and the dispersion of pollutants in littoral zones [7].

1-2 Tropical storm

Tropical cyclones represent one of the most significant and destructive meteorological phenomena in tropical and subtropical regions. They are distinguished by a closed low-level atmospheric circulation, intense wind fields, and a spiral configuration of convective thunderstorms accompanied by heavy precipitation. Their defining characteristic lies in the concentration of thermal energy extracted from warm ocean surfaces and its subsequent conversion into powerful winds and torrential rainfall [8].

The nomenclature of these systems varies according to the ocean basin in which they occur. In the North Atlantic and the Northeast Pacific, they are referred to as hurricanes; in the Northwest Pacific, they are termed typhoons; and in the Indian Ocean and the South Pacific, they are designated as tropical cyclones [25]. This distinction in terminology is purely geographical, as their underlying dynamical structure and physical characteristics remain fundamentally similar across all regions.

On average, between 80 and 90 tropical cyclones develop globally each year, approximately half of which intensify to the stage where sustained wind speeds exceed 65 knots (≈120 km/h) [20]. Beyond their destructive impacts, tropical cyclones play a pivotal role in the meridional transport of heat and energy from tropical to higher latitudes, thereby functioning as integral components of the global climate-regulating system.

The study of tropical cyclones is of critical importance not only because of their profound human and economic impacts but also due to their central role in the hydrological cycle, atmospheric moisture transport, and climate variability. In recent decades, rising sea surface temperatures and ongoing global climate change have heightened concerns regarding the intensity and frequency of these systems, making them a central focus of contemporary research in climatology and oceanography [18].

Tropical cyclones predominantly develop over extensive tropical oceanic regions where sea surface temperatures exceed 26–27 °C. Such thermal conditions promote intense evaporation from the ocean surface, generating substantial amounts of water vapor. As this vapor ascends through the atmosphere and reaches the condensation level, it undergoes phase change, releasing latent heat. This release of energy constitutes the primary driving mechanism of the cyclone, intensifying convective activity, fostering the development of cumulonimbus cloud systems, and producing heavy precipitation [8].

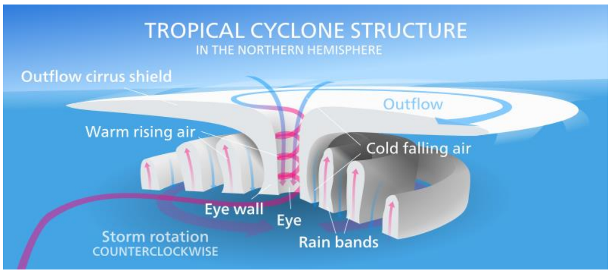

Figure 1. Schematic representation of the structural features of tropical cyclone formation in the Northern Hemisphere

This energy source is fundamentally distinct from that of mid-latitude cyclones, which are primarily driven by horizontal temperature gradients associated with frontal systems, such as cold and warm fronts. By contrast, tropical cyclones operate as heat-engine

systems that extract their energy directly from the ocean surface through the release of latent heat [11].
Tropical cyclones typically exhibit diameters ranging from 100 to 2,000 km, with their intensity largely governed by prevailing environmental conditions. The strong rotational winds characteristic of these systems arise from the conservation of angular momentum induced by the Earth's rotation, commonly referred to as the Coriolis Effect. Consequently, cyclone genesis is exceedingly rare within latitudes lower than 5°, where the Coriolis force is negligible; nevertheless, a few exceptional cases have been documented historically [20].
From a geographical perspective, the spatial distribution of tropical cyclones varies considerably across ocean basins. In the South Atlantic Ocean, their occurrence is extremely rare due to the combined influence of strong vertical wind shear and the weak development of the Intertropical Convergence Zone (ITCZ), both of which inhibit cyclone formation. By contrast, in the North Atlantic Ocean and the Caribbean Sea, the presence of the East African Jet and its associated atmospheric instabilities creates favorable conditions for cyclone development [5].

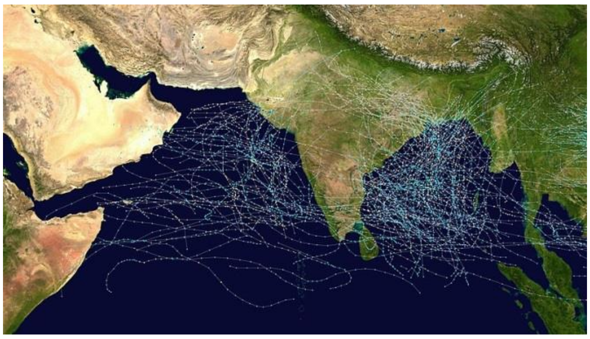

Figure 2. Historical tracks of tropical cyclones in the North Indian Ocean during the period 1970–2020

During tropical cyclones, the behavior of surface waves exerts a direct influence on maritime safety, structural stability, and coastal operations. The severe wave fields generated by these systems can inflict substantial damage on shipping activities, disrupt international trade routes, and endanger critical coastal and offshore infrastructure. Consequently, a precise understanding of wave dynamics under cyclonic conditions is essential for forecasting marine hazards and for the development of effective early-warning and risk-reduction strategies. In this context, the primary objective of the present study is to investigate and analyze the evolution of surface waves during Cyclone Asna (2024) in the northern Indian Ocean and the Arabian Sea. To achieve this, a coupled wave–atmosphere modeling framework (WRF–WWIII) is employed to simultaneously simulate wind fields and wave responses, thereby providing a realistic representation of wave intensity and temporal evolution throughout the cyclone's lifecycle. This integrated approach enables a more accurate assessment of navigational conditions under extreme wave regimes and offers a scientific basis for enhancing maritime safety and risk management in high-vulnerability marine regions.

2. Research Method

2-1 Numerical Atmospheric-Ocean Modeling

Numerical modeling in atmospheric and oceanic sciences has emerged as a cornerstone of research and forecasting in the field of natural hazards over recent decades. These models enable the accurate representation of complex environmental processes by solving the governing equations of geophysical fluid dynamics, thermodynamics, and the mechanisms of energy and mass exchange between the atmosphere and the ocean. Advances in computational capacity and the refinement of numerical algorithms have transformed these models from relatively simple frameworks into high-resolution, three-dimensional coupled systems capable of simultaneously simulating interactions among atmospheric layers, the sea surface, and subsurface oceanic structure [2].
The applications of such models in meteorology and oceanography are extensive, ranging from short-term forecasts of weather and marine conditions on daily timescales to long-term simulations of climate variability and change over multi-decadal horizons. By integrating observational datasets with fundamental physical laws, these models are able to reconstruct nonlinear feedbacks, dynamic instabilities, and large-scale climate phenomena such as the El Niño–Southern Oscillation (ENSO) and the Indian Ocean monsoon [16].
In the present study, given the strategic importance and complex dynamics of the North Indian Ocean and the Arabian Sea, as well as the critical dependence of shipping, navigation, and trans-regional operations on accurate sea-state predictions, the objective was to develop a coupled atmosphere–ocean modeling framework with high accuracy and scientific robustness. To this end, existing numerical models were systematically reviewed and evaluated in terms of their strengths and limitations, and a selected framework was adapted to simultaneously represent atmospheric and oceanic components. As a case study, Cyclone Asna (2024) was simulated using the coupled WRF–WWIII system to assess the model's capability in reproducing the dynamic and thermodynamic characteristics of the storm and in predicting associated sea-state conditions.

2-2 WRF Numerical Atmospheric Model

The Weather Research and Forecasting (WRF) model is a state-of-the-art mesoscale numerical weather prediction system developed to address the expanding requirements of atmospheric research and environmental forecasting. It incorporates multiple dynamical cores, a three-dimensional variational (3DVAR) data assimilation framework, and a software architecture designed for parallel computation and scalability. Owing to its versatility, WRF is applicable across a broad spectrum of meteorological studies, spanning spatial scales from a few meters to several thousand kilometers. The development of WRF has been the result of a collaborative effort involving multiple institutions and research centers, including the National Center for Atmospheric Research (NCAR), the National Oceanic and Atmospheric Administration (NOAA), and other academic and governmental partners.

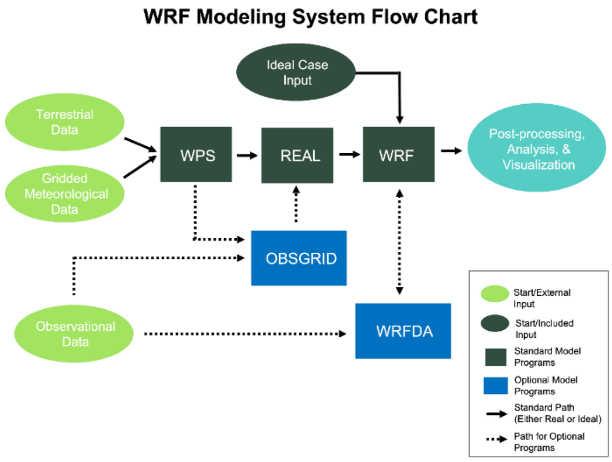

Figure 3. Schematic representation of the modeling execution process in the Weather Research and Forecasting (WRF) model

By default, the Weather Research and Forecasting (WRF) model is a fully compressible, non-hydrostatic numerical framework that employs a hybrid vertical coordinate (HVC) system based on hydrostatic pressure and utilizes an Arakawa C-grid staggering. The model incorporates second- and third-order Runge–Kutta time integration schemes, along with second- to sixth-order advection schemes in both horizontal and vertical dimensions. A reduced time step is applied for acoustic and gravity wave modes to ensure numerical stability.

The WRF modeling system includes several executable components: an initialization program for real-data simulations (real.exe) and for idealized cases (ideal.exe); a numerical integration program (wrf.exe); and a one-way nesting utility (ndown.exe) that enables the simulation of nested domains independently. The Advanced Research WRF (WRF-ARW) core employs a dynamical solver to perform spatial and temporal integration of the governing equations of motion. These equations are advanced forward in time to generate forecasts. Since analytical solutions are not feasible, the equations are discretized on a computational grid to obtain approximate numerical solutions, with the accuracy of results depending on both the numerical schemes employed and the grid resolution.

2-3 Numerical Model of WWIII Waves

The development of numerical wave models over recent decades has traced a significant evolutionary trajectory in coastal engineering and physical oceanography. First-generation models were largely based on one-dimensional energy spectra and frequency-domain energy-transfer formulations. Due to substantial geometric and physical simplifications, these early systems could estimate only basic parameters—such as significant wave height and characteristic periods—and were of limited utility in complex marine environments [12].

Second-generation models introduced energy transfer in two-dimensional spectral space (frequency–direction) and incorporated selected nonlinear processes. This enhanced their capacity to represent wind-sea growth and swell propagation, thereby improving operational forecasting skill. Nevertheless, key physical mechanisms were still not fully captured, constraining their realism under diverse forcing conditions [17].

A major inflection point arrived with third-generation models, which solve the wave kinetic (Boltzmann-type) equation in two-dimensional spectral space without prescribing the spectral shape. By explicitly representing core processes—wind-wave growth, nonlinear triad and quartet interactions, breaking-induced dissipation, and frictional losses—these models deliver substantially improved skill across a wide range of sea states [22].

These advances culminated in global reference systems such as WAM and WAVEWATCH III, now foundational tools for operational wave forecasting and climate applications. Notably, WAVEWATCH III has extended applicability from the open ocean to nearshore zones by incorporating observation-informed source terms and improving the representation of coastal processes, thereby enhancing performance in complex bathymetric and meteorological settings [14].

The WAVEWATCH III (WW3) numerical model stands among the most consequential achievements in modern wave modeling and has been widely adopted by research and operational centers since the early 1990s. Building on the lineage of first-generation WW I models developed at Delft University and second-generation WW II systems designed by NOAA, WW3, as a third-generation framework, solves the kinetic equation without imposing a priori spectral forms, enabling accurate resolution of the two-dimensional frequency–direction spectrum [23]. Developed at the Environmental Modeling Center under NCEP stewardship, WW3 has progressively integrated new capabilities and now supports simulations from global basins to coastal and nearshore domains.

2-4 Tropical Storm ASNA

Tropical Cyclone Asna, which occurred between 25 August and 2 September 2024, represents one of the most significant cyclonic events in recent years in the northern Indian Ocean and the Arabian Sea. The system initially developed as a deep depression over northwestern India and, under favorable thermodynamic and dynamic conditions with sustained moisture supply, intensified into a cyclonic storm before tracking westward into the Arabian Sea [10].

The cyclone produced torrential rainfall that triggered widespread flooding across Gujarat, India, and Sindh, Pakistan. Official reports documented at least 49 fatalities in India and 24 in Pakistan, alongside extensive damage to public infrastructure, private property, and agricultural lands. Preliminary assessments estimated the total economic losses at approximately USD 30 million.

From a dynamical perspective, the genesis and intensification of Asna were strongly influenced by persistent easterly winds over the southern Indian subcontinent, in conjunction with a Boreal Summer Intraseasonal Oscillation (BSISO) event. These conditions fostered the development of a low-pressure system that subsequently evolved into a full depression.

This dynamical–thermodynamic interaction provides a clear example of the coupling between large-scale monsoonal processes and local surface–atmosphere feedbacks in the formation and evolution of tropical disturbances. Such mechanisms are of particular importance for advancing the understanding of cyclone life cycles in the region and for improving the skill of numerical modeling frameworks [15].

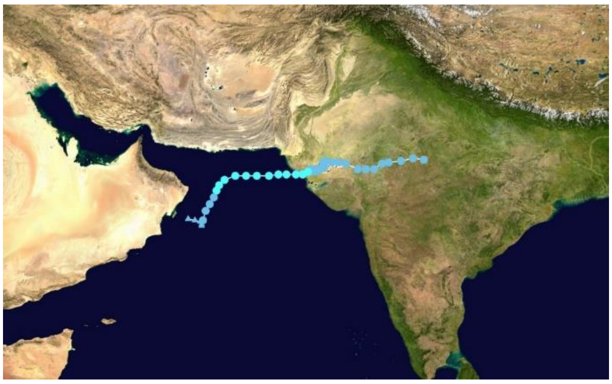

Figure 4. Track of Cyclone Asna (25 August – 2 September 2024) across the Arabian Sea

3 Coupled Numerical Modeling

The coupled atmosphere–wave modeling capability within the COAWST framework is among the most advanced approaches for simulating coastal and offshore dynamics. By enabling two-way, synchronous exchange between the WRF atmospheric model and the WWIII wave model, the system represents complex air–sea feedbacks with high realism. This coupling captures how evolving wave fields modulate the atmospheric boundary layer and, in turn, how atmospheric forcing shapes the wave spectrum and energy distribution [24].

In this architecture, atmospheric variables—including wind fields, sea-level pressure, and surface heat fluxes—are passed to the wave model. Conversely, wave parameters such as significant wave height, dominant period, and wavelength feed back to the atmosphere via their impact on sea-surface roughness and momentum exchange. The data exchange is handled through a coupler with configurable coupling frequency, allowing feedback effects to be computed and updated dynamically at each time step. This ensures that transient interactions during rapidly evolving events, such as cyclones, are resolved consistently across both model components [6].

The importance of this coupling is pronounced during high-impact atmosphere–ocean phenomena—tropical storms, tropical cyclones, and monsoons—where wave conditions can directly reshape the structure of the atmospheric boundary layer and modulate wind intensity. For example, increases in wave height and shifts in spectral energy can elevate effective surface roughness and alter the drag coefficient, thereby changing momentum transfer from the atmosphere to the ocean. Ignoring these pathways in uncoupled systems can introduce substantial errors in predicting storm intensity and track, and in assessing marine hazards [9].

3-1 WRF Atmospheric Model Configuration

The WRF domain configuration in the WPS preprocessing stage employs a nested setup to resolve both synoptic-scale circulation and fine-scale features with appropriate fidelity.

Parent domain (d01): Covers a broad region spanning parts of West Asia, the Arabian Sea, the northern Indian Ocean, and South Asia. The objective is to capture large-scale synoptic patterns and the primary drivers influencing the target area. A coarser grid spacing (15 km) supports numerically stable, computationally efficient simulations while providing high-quality boundary and initial conditions to inner nests.

Child domain (d02): Encompasses a smaller, high-priority area including the Arabian Sea, India's western coastline, and segments of the Arabian Peninsula. Configured at higher resolution (5 km) to resolve extreme wind gradients, cyclone inner-core structure, coastal topographic influences, and local variability relevant to Cyclone Asna. High-resolution wind fields from d02 are directly supplied to the WWIII model within the COAWST framework, furnishing detailed forcing and boundary conditions for wave simulations and improving representation of storm-driven wave dynamics.

This nested strategy balances computational efficiency with physical realism, ensuring that synoptic-scale drivers are consistently propagated inward while local processes critical to cyclone evolution and coastal impacts are explicitly resolved.

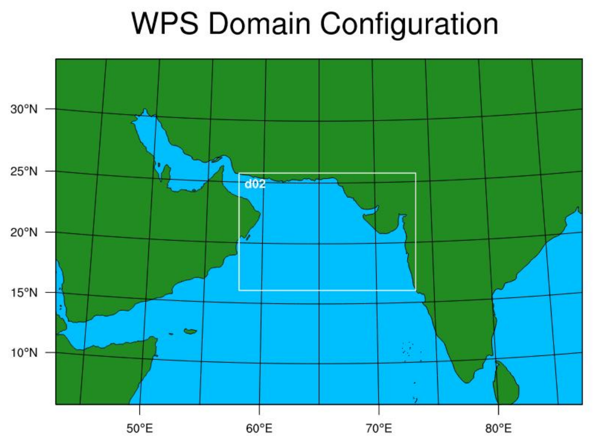

Figure 5. Configured domains of the WRF atmospheric model used in this study

The outer domain computational grid comprises 270 points along the east–west axis (e_we) and 180 points along the north–south axis (e_sn). Combined with a horizontal resolution of 15 km (dx = dy = 15,000 m), this configuration provides complete coverage of the study region with appropriate fidelity. The chosen grid dimensions and spacing reflect a balance between accuracy and computational cost, ensuring sufficient detail for local analyses while maintaining numerical stability and efficiency.

To represent vertical atmospheric processes, the model employs 45 vertical levels (e_vert). This level count affords adequate vertical resolution to resolve the atmospheric boundary layer, the middle and upper troposphere, and the associated dynamical and thermodynamical processes. The model top pressure is set to 5,000 Pa, corresponding to an altitude of approximately 20 km, thereby encompassing the full troposphere and a portion of the lower stratosphere. This selection is crucial for correctly representing vertical interactions and energy transfer among atmospheric layers, particularly during extreme weather events.

In this configuration, lateral boundary conditions are enabled (specified = .true), indicating that boundary data are ingested from external files and applied to the model. Boundary and initial conditions for the outer domain are prepared from global forecast products with suitable coverage and temporal–spatial resolution (e.g., wind, temperature, humidity, pressure, and geopotential height at multiple levels). This approach ensures an accurate depiction of large-scale atmospheric patterns that modulate the target region.

The boundary data input interval is set to 21,600 seconds (6 hours), consistent with common global forecast and reanalysis update cycles. Regular updates during multi-day simulations help minimize model drift and sustain coherence with evolving real-world conditions, which is particularly important for capturing synoptic variability and cyclone-related dynamics.

The outer-domain horizontal grid comprises 270 × 180 points with a 15 km resolution (dx = dy = 15,000 m). This configuration balances broad regional coverage with spatial fidelity, enabling simultaneous simulation of synoptic-scale circulation and locally relevant features. It allows the model to capture long-range influences of atmospheric systems while resolving dynamic details within the target region.

In the vertical, the model employs 45 levels extending from the surface to a model-top pressure of 5,000 Pa. This affords adequate vertical resolution to represent the atmospheric boundary layer and the middle–upper troposphere. Such resolution is essential for resolving dynamical and thermodynamical processes—vertical convection, turbulent mixing, and energy transfer between layers—particularly under severe weather conditions.

To rigorously assess the impact of wind-data quality and origin on simulations of extreme events over oceanic domains, two independent datasets are used for initial and lateral boundary conditions.

First dataset: NCEP GFS operational analysis. Produced on a frequent operational cycle with short latency, providing up to 240-hour forecasts. Its strength lies in supporting short-term, time-critical applications; however, limitations in spatiotemporal resolution and evolving system configurations can reduce fidelity in reproducing fine-scale inner-core structures and peak wind intensities of tropical cyclones.

Second dataset: GFS global analysis/reanalysis. A homogeneous, high-quality product with ~0.25° resolution that integrates diverse observations (satellite, buoy, and station). It more accurately reconstructs wind fields and pressure gradients during extremes, offering improved representation of tropical cyclones in the northern Indian Ocean and Arabian Sea.

The lateral boundary update interval is set to 21,600 seconds (6 hours), aligning with common global data cycles and ensuring regular refresh of the outer domain. This schedule mitigates model drift in multi-day simulations and maintains coherence with evolving real-world synoptic conditions.

3-2 WWIII Wave Model Configuration

In the present configuration, the computational domain of the WAVEWATCH III (WW3) model is designed to fully encompass the northwestern Indian Ocean and the Arabian Sea. This domain selection is critical for analyzing wind–wave interactions associated with monsoonal circulation and trans-regional wind systems that dominate this basin.

A structured, rectangular grid is employed to facilitate the spectral solver's implementation of wave energy transfer equations and associated source terms within a regular coordinate framework. This design ensures numerical simplicity, computational efficiency, and stability in the solution of the spectral action balance equation. Moreover, the structured grid configuration enhances the efficiency of online coupling with the atmospheric model by providing consistent spatial alignment. This alignment improves the accuracy of input–output parameter mapping—particularly for 10 m wind fields and surface roughness—while minimizing interpolation errors that often arise in irregular or unstructured grids.

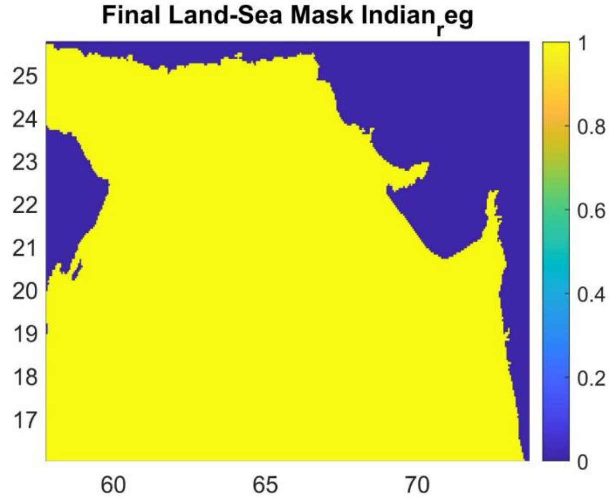

Figure 6. Computational scope of the WAVEWATCH III (WWIII) wave model applied in this study

The computational grid comprises 319 points in longitude (east–west) and 196 points in latitude (north–south). A uniform horizontal resolution of 0.05° is adopted in both directions, equivalent to approximately 5 km by conventional approximation; however, the effective zonal spacing varies slightly with latitude, while the meridional spacing remains nearly constant. This spatial fidelity provides an optimal resolution for wave dynamics in the target basin while maintaining a favorable balance between accuracy and computational cost for a regional spectral model. From a numerical stability standpoint, the chosen resolution supports an acceptable time step for solving spectral transport and wind–wave interactions and mitigates stringent stability constraints, particularly under two-way coupling with the atmospheric model.

The southwestern corner of the domain is positioned at 58°E, 16°N. Given the grid dimensions and resolution, the horizontal extent spans approximately 16° in longitude and 10° in latitude, placing the northeastern corner near 74°E, 26°N. This layout ensures inclusion of key sectors of the northern Indian Ocean and preserves dynamical connectivity between coastal margins and offshore waters. The geographic bounds also enable a rational design of open boundary conditions, facilitating exchange of spectral energy with external systems without inducing numerical reflections or artificial spectral damping. The wave-model domain and grid are co-designed to be consistent with the atmospheric modeling d02 nest in both dimensions and regional coverage, reducing systematic errors from wind-field interpolation into the wave model.

A rectangular, structured grid of these dimensions yields practical implementation advantages: streamlined land–sea masking; unambiguous application of seabed bathymetry; direct ingestion of co-scale wind and sea-level pressure fields from the atmospheric model (or precise linear interpolation when needed); and synchronized execution with WRF to support hourly or sub-hourly exchange of key parameters. Consequently, wave–atmosphere feedbacks are applied consistently across the coupling cycle, and the wind fields driving wave growth evolve dynamically throughout the simulation. This amplitude and resolution configuration establishes the prerequisites for reproducing regional spectral properties and for assessing the wave system's sensitivity to changes in wind forcing, coastal geometry, and bed roughness.

Seabed data are provided by the GEBCO global bathymetry database, an open and up-to-date source of regular depth grids at global scale. Compiled from direct hydrographic measurements and satellite-derived estimates, these data support accurate representation of seabed topography in the northern Indian Ocean. Incorporating GEBCO bathymetry into WW3 is pivotal for simulating propagation, refraction, and interference, because depth variations directly influence phase speed, refraction, and energy dissipation—especially across coastal and continental-shelf regions. The dataset was obtained in regular-grid format with suitable spatial resolution and, after spatial subsetting to the study area, applied as input to the model's bathymetric layer [26].

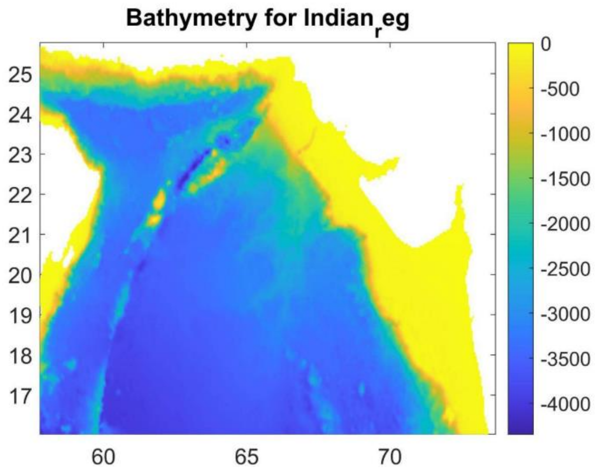

Figure 7. Bathymetry of the computational domain used for wave modeling, extracted from the GEBCO global bathymetric database

In the present wave modeling, the physical configuration of the WW3 model employs the ST3 physics package, a widely validated scheme for regional and global wind-wave simulations [19]. ST3 provides optimized formulations for the key processes governing wave growth, dissipation, and interspectral energy transfer, and is particularly suitable for online coupling with atmospheric models such as WRF due to its consistent treatment of air–sea fluxes and boundary-layer sensitivities.

For wind input, the Tolman–Chalikov formulation is activated under the SIN3 option. This approach computes the energy transfer rate from the atmosphere to the wave field based on atmospheric boundary-layer parameters and spectral characteristics of the waves [21]. The setting ZWND = 10 specifies that the model ingests wind at the standard 10 m reference height above mean sea level, ensuring physically consistent calculation of wind stress and wave growth. This choice is especially important under strong-wind regimes, where sensitivity to the reference height materially affects the accuracy of momentum and energy exchanges.

Energy dissipation due to whitecapping is represented with the SDS3 parameterization, selected for consistency with the chosen wind-input scheme [21]. Whitecapping—local breaking near wave crests—is a primary deep-water dissipation mechanism that shapes the spectral energy distribution. The SDS3 formulation links dissipation rates to spectral properties and wind intensity, establishing a dynamic balance between growth and attenuation. In practice, the effective intensity of whitecapping is among the key calibration levers for aligning modeled significant wave heights with field observations.

Nonlinear interspectral energy transfer is treated with the discrete interaction approximation under the SNL1 option. This method captures energy exchanges among spectral components at comparatively low computational cost while preserving the essential physics of downshift and upscale transfers across frequency bands [1]. The scaling factor NLPROP = 3.0×10^7 modulates the rate and strength of these transfers, thereby influencing the evolution of the spectral shape and the distribution of energy among peaks and tails.

Bottom friction is parameterized using the JONSWAP-based SBT1 scheme with GAMMA = −0.038. This formulation is particularly relevant in shallow and shelf waters, where momentum exchange with the seabed induces energy loss and modifies wave heights. The GAMMA setting controls dissipation intensity and directly impacts coastal predictions, especially across continental-shelf regions where bathymetric gradients and roughness strongly influence wave transformation [3].

3-3 Coupled Modeling Configuration

The WRF atmospheric model configuration (including the physical schemes of the planetary boundary layer, fine-scale convection, and the exchange of surface fluxes), along with the spectral and numerical settings of the WW3 wave model and the precise definition of the exchange variables in the namelist and coupling files, was implemented and executed in the COAWST framework. This structure allows for a two-way and dynamic exchange between the atmospheric and wave components and ensures that mutual feedbacks at each time step are accurately considered in the simulation.

In particular, the selection of physical schemes in WRF and the implementation settings in the WW3 model were made based on validated studies in the Indian Ocean and the Arabian Sea. These choices ensure that the present modeling is capable of representing the real wind and wave conditions in the region and that its results can be used in both scientific and applied analyses.

In the present modeling, the coupling of the atmospheric and wave models in the COAWST framework was configured using the MCT tool in such a way that the two-way exchange of variables was carried out dynamically and simultaneously at each time step. In this structure, atmospheric data—including surface wind at a reference height of 10 m and sea level pressure—were transferred to the wave model to represent the process of wave growth and evolution under the direct influence of the wind field. Conversely, wave outputs—including sea surface roughness, wave momentum flux, and changes in the surface friction coefficient—were returned to the atmospheric model to account for the feedback effect of waves on the atmospheric boundary layer structure and wind intensity. The temporal synchronization of these exchanges was carried out with a common time step of 360 seconds, which ensured numerical stability and dynamic coherence in the simulation. The main goal of this coupling was to accurately represent and predict the atmosphere–wave conditions during Cyclone Asna (2024) in the northwest Indian Ocean.

4. Results and Discussion

In this section, the results of the coupled atmosphere–wave numerical simulations using the WRF and WWIII models to reproduce Tropical Cyclone Asna (2024) in the northern Indian Ocean are presented and analyzed. Unlike fully coupled atmosphere–ocean–wave systems, this study focuses exclusively on the two-way interactions between the wind field and surface waves, while the ocean circulation component (e.g., ROMS) is not included in the model configuration. The primary objective is to evaluate the capability of the coupled WRF–WWIII system in reproducing the dynamical characteristics of the cyclone, particularly the wind structure and significant wave height along its track, using reliable reanalysis data as a reference.

Due to the absence of in situ measurements such as buoy and field observations in the study area, the validation of the WWIII wave model outputs was carried out solely against ERA5 reanalysis data provided by the European Centre for Medium-Range Weather Forecasts (ECMWF). Model performance was assessed along the storm track and at selected time intervals by comparing significant wave height (Hs) and dominant wave direction with ERA5 results. In addition, the surface wind field predicted by the

WRF model was evaluated against ERA5 to examine the accuracy of the model in representing the intensity and spatial structure of the wind during storm conditions.

3-1 Evaluation of Incoming Wind Fields

As mentioned in the previous section, to investigate and compare the performance of different wind sources in simulating tropical cyclone events, two independent datasets were employed as the initial and boundary conditions of the atmospheric model: (1) the 240-hour global operational forecast data from NCEP GFS, and (2) the global reanalysis data from GFS. The purpose of this approach was to comparatively assess the accuracy of global short-range forecast data against homogeneous and high-quality reanalysis data in reproducing wind characteristics and boundary conditions associated with tropical cyclones in the northern Indian Ocean. This comparison provided insight into the extent to which the quality and source of wind data influence the prediction of key parameters of the wave system and storm intensification.

The modeling results indicate that the GFS reanalysis data performed better than the GFS forecast data in representing the intensity of Cyclone Asna during its passage through the Arabian Sea. This improvement in atmospheric forcing directly enhanced the accuracy of the wave simulations when GFS reanalysis data were used as boundary inputs to the WRF model.

To further analyze the dynamic behavior of Tropical Cyclone Asna during its initial stage and subsequent development over India, two-dimensional wind field maps at 10 m above the surface were generated. These maps were produced at 12-hour intervals from 00:00 UTC on August 26, 2024, to 18:00 UTC on August 30, 2024, allowing the temporal evolution of wind intensity and direction along the storm track to be examined in a continuous and structured manner. The analysis focuses on identifying surface convergence patterns, regions of maximum wind speed, and the spatial expansion of the wind field relative to the storm center—factors that play a critical role in assessing coastal and marine hazards. The maps were derived from the coupled WRF–WW3 model outputs and validated against ERA5 reanalysis data to ensure reliability.

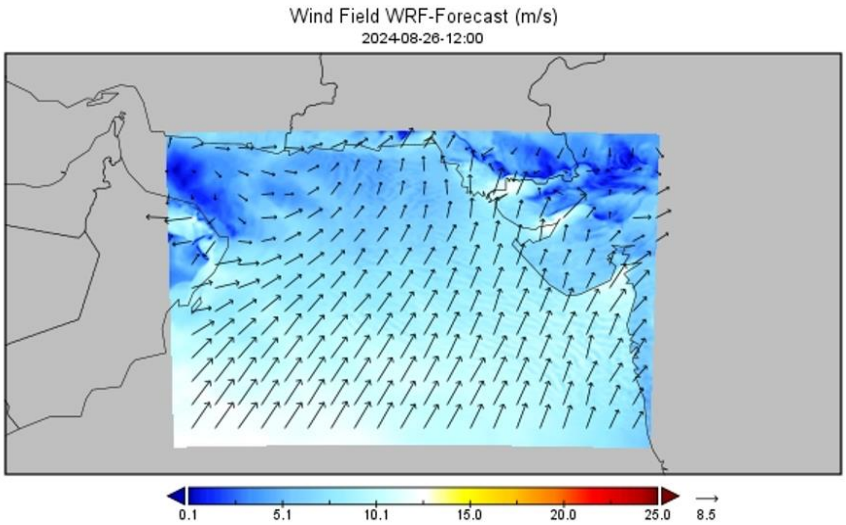

Figure 8. Results of WRF wind field modeling with GFS forecast input data at 12:00 on 08/26/2024

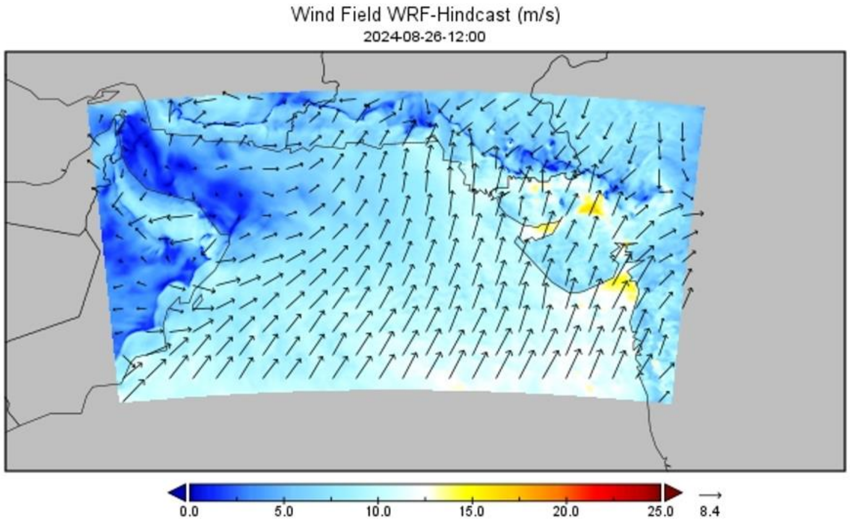

Figure 9. Results of WRF wind field modeling with GFS reanalysis input data at 12:00 on 08/26/2024

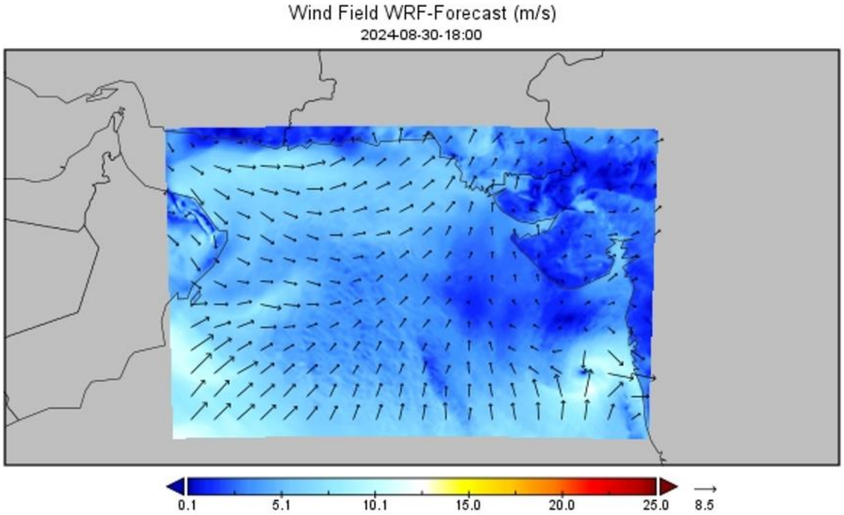

Figure 10. Results of WRF wind field modeling with GFS forecast input data at 18:00 on 08/30/2024

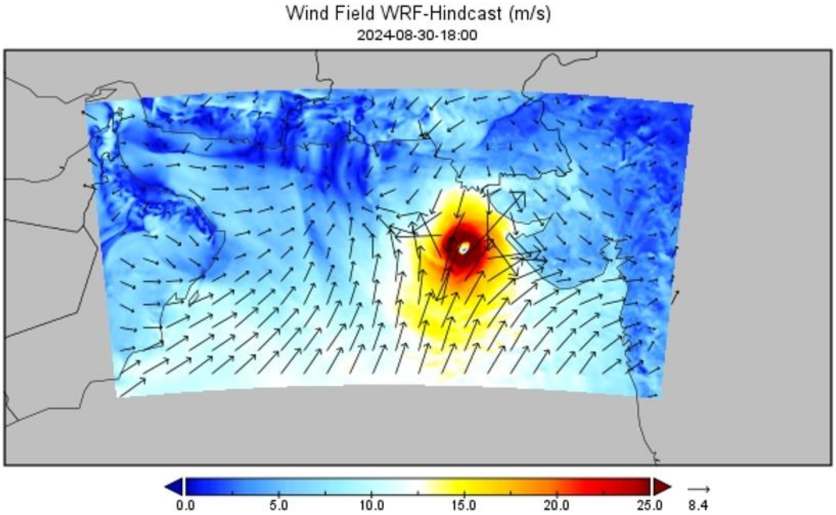

Figure 9. Results of WRF wind field modeling with GFS reanalysis input data at 18:00 on 08/30/2024

3-2 Assessment of Significant Wave height

The validation process of the numerical modeling of Cyclone Asna focuses on evaluating the wave height outputs from the WWIII model, which was forced with different surface wind datasets. Since the surface wind field plays a decisive role in the generation and transfer of energy to the sea surface, the quality and structure of the input wind data have a direct impact on the accuracy of wave height simulations. In this study, two wind datasets— GFS forecast and GFS reanalysis —were used separately to drive the WWIII wave model in order to investigate their structural and functional differences in reconstructing cyclone-induced waves.

The WWIII model was run from August 26 to 30, 2024, with wave height outputs extracted at hourly intervals. This period encompasses the initiation, intensification, and mature stages of Cyclone Asna, which exerted significant influence over the northern Indian Ocean and the western coast of India in the Arabian Sea. The purpose of this evaluation is to assess the accuracy of the model in representing maximum wave height, the spatial structure of the wave field, and the temporal agreement with observational or reanalysis data. In addition, comparing outputs generated from different wind inputs provides insight into which dataset is more suitable for wave modeling under storm conditions.

Based on the results obtained in the wind field analysis, it is anticipated that GFS data will perform better in generating extreme waves due to its more accurate spectral representation and higher resolution. In contrast, GFS forecast data are expected to produce underestimated wave heights, primarily because of their weaker representation of the pressure gradient and surface convergence.

3-2-1 Time Series Charts

In numerical studies of tropical cyclones and maritime operations, accurate evaluation of significant wave height (SWH) is a fundamental requirement for validating wave models such as WWIII. Considering the vast geographical extent of the Arabian Sea and the limited availability of in situ observations, including active wave buoys, the use of wave reanalysis products such as ERA5 provides a reliable and scientifically sound reference for model evaluation. The ERA5 dataset, produced by ECMWF, offers global wave simulations with high spatial resolution and hourly temporal resolution, based on the IFS–WAM wave model.

In the present study, ERA5 data were extracted at the locations indicated in the map below to examine the time series of SWH at key points along the track of Tropical Cyclone Asna. These points, situated in both central and coastal regions of the Arabian Sea, were selected to represent the wave field at different stages of the storm, including wind convergence zones, areas of maximum surface wind energy, and regions directly impacted by the cyclone. ERA5 data at these locations served as the reference for comparison with WWIII model outputs forced by different wind inputs (forecast and reanalysis).

Analyzing the wave time series at these points enables a detailed assessment of the growth, peak, and decay phases of storm-induced waves. Furthermore, by evaluating the temporal correspondence and amplitude of wave oscillations between ERA5 and the model outputs, the performance of each model configuration in reproducing wave dynamics can be systematically assessed. This approach provides an effective means of indirect model validation and supports the optimal selection of input wind datasets, particularly in regions where direct observational data are unavailable. In the following, the time series plots of SWH at the selected points are presented, and the structural differences between the simulations are analyzed both quantitatively and qualitatively.

To evaluate the performance of the WWIII wave model in reconstructing the significant wave height of Hurricane Asna, time series plots were prepared at key points along the storm track. These plots present the model outputs under two different configurations (with GFS forecast and GFS reanalysis input wind data) alongside ERA5 wave reanalysis data as a reference for comparison. The purpose of this comparison is to examine the temporal accuracy and amplitude of wave oscillations in each configuration, analyze the maximum wave height, and evaluate the model's capability in reproducing the growth and attenuation of storm-induced waves during the modeling period.

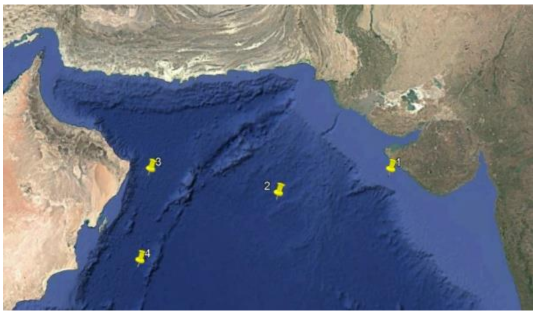

Figure 10. Locations of the assessed significant wave height (SWH) points along the track of Tropical Cyclone Asna in the northern Indian Ocean

Table 1. Geographical locations of the assessed significant wave height (SWH) points along the track of Tropical Cyclone Asna in the northern Indian Ocean

Location		*Station*
Long.	*Lat.*	*No.*
69	*21.5*	*1*
65	*21*	*2*
60.5	*22*	*3*
60	*19*	*4*

Given the structural differences in the input wind fields, the model outputs using GFS data are expected to show greater consistency with ERA5, particularly in the central regions of the storm and along the coastal areas. These plots form the basis for the quantitative and qualitative analyses in the next section and contribute to identifying the optimal input data source for wave modeling under storm conditions.

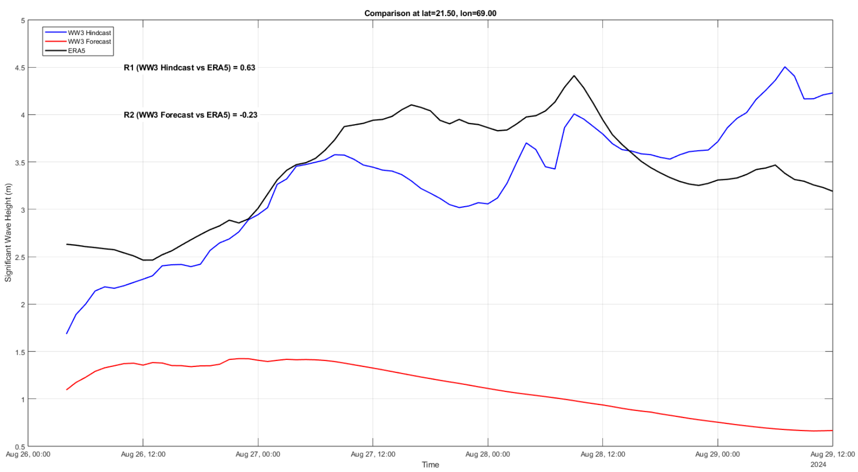

Figure 11. Time series of significant wave height (SWH) at index station 1 during Tropical Cyclone Asna

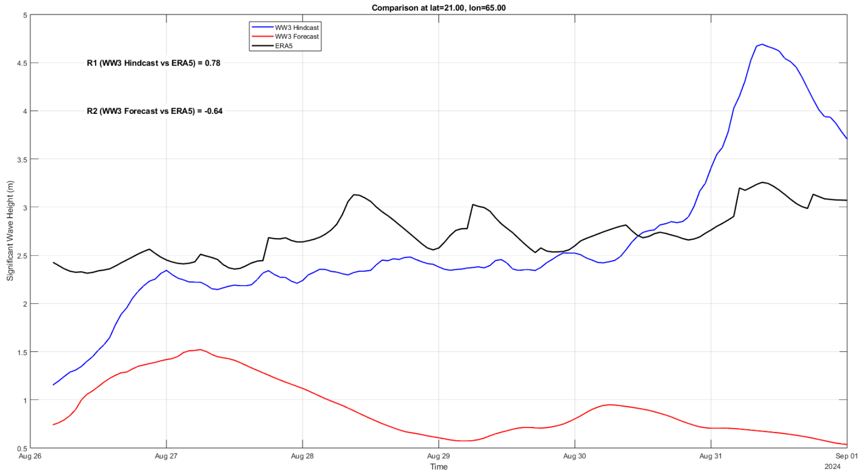

Figure 12. Time series of significant wave height (SWH) at index station 2 during Tropical Cyclone Asna

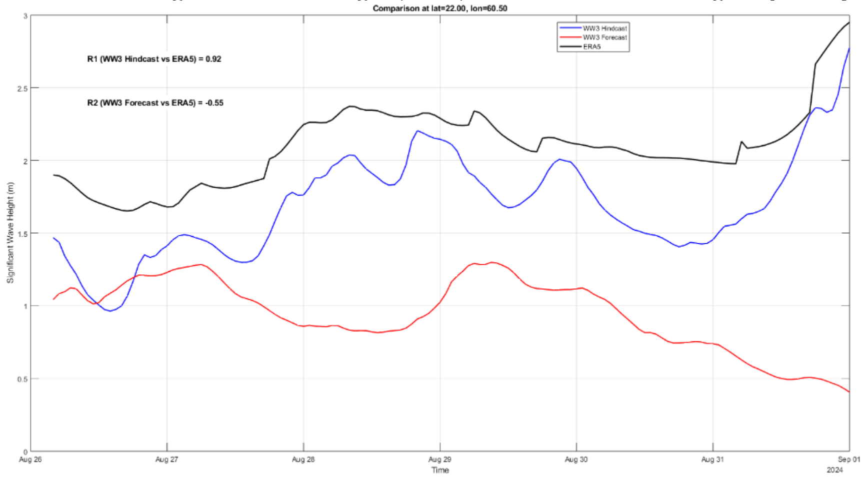

Figure 13. Time series of significant wave height (SWH) at index station 3 during Tropical Cyclone Asna

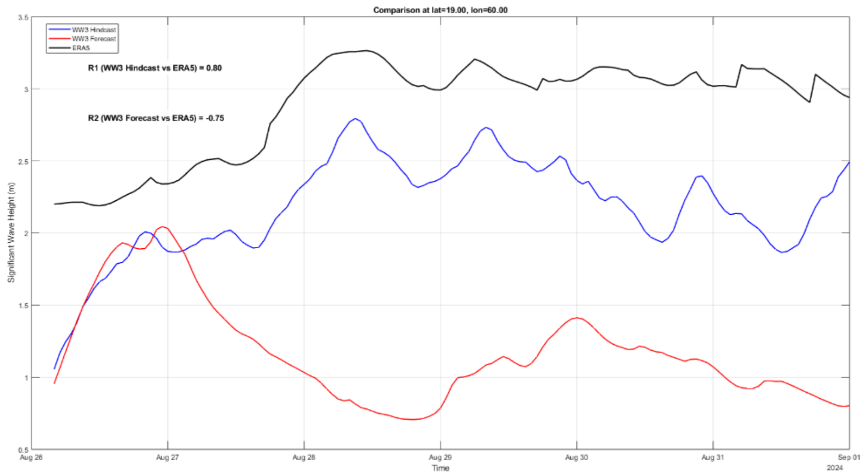

Figure 14. Time series of significant wave height (SWH) at index station 4 during Tropical Cyclone Asna

The analysis of the time series of significant wave height (SWH) at four selected stations during Cyclone Asna (2024) in the Arabian Sea provides a comprehensive assessment of the performance of the WW3 model under different wind datasets, compared with ERA5-Wave reference data.

At station 1, located in the northwestern Arabian Sea near the Gujarat coast, the wave growth trend began on 26 August and reached a peak of about 4.2 m in ERA5 on 28 August. The WW3 model reproduced this trend with acceptable accuracy using GFS data, producing a maximum of about 3.8 m, which was consistent with ERA5 in terms of timing and overall structure. In contrast, the forecast data resulted in a lower maximum (2.5 m) and unrealistic fluctuations. The correlation coefficient (R) at this station was 0.63 for GFS and –0.23 for GFS forecast, indicating the clear superiority of GFS in representing coastal wave conditions.

At station 2, located in the central Arabian Sea and directly in the storm's path, ERA5 recorded a maximum of about 3.2 m. The WW3 model with GFS data reproduced this trend with high accuracy, simulating a maximum of about 4.5 m, while the forecast data produced only 1.5 m and showed inconsistent peak timing. The correlation coefficient was 0.78 for GFS reanalysis and –0.64 for GFS forecast. These results indicate that in central and high-energy regions, GFS data have a greater ability to transfer wind energy to waves.

At station 3, located in the northwestern Arabian Sea near the coast of Oman, ERA5 showed a maximum of about 2.9 m. The WW3 model with GFS data reproduced this value with a maximum of about 3.6 m and accurate timing, while the forecast data simulated only 1.6 m. The correlation coefficient at this station was 0.92 for GFS reanalysis and –0.55 for GFS forecast. These findings demonstrate that even in semi-coastal and marginal areas, GFS reanalysis data perform much better than GFS forecast.

At station 4, located in the southeastern Arabian Sea and farther from the storm center, ERA5 recorded a calmer wave trend with a maximum of about 2.3 m. The WW3 model with GFS data reproduced this trend with a maximum of about 2.8 m and good timing, while the forecast data simulated only 2.1 m with scattered fluctuations and irregular timing. The correlation coefficient at this station was 0.80 for GFS reanalysis and –0.85 for GFS forecast.

Overall, the results from the four stations show that GFS data, across all locations—coastal, semi-coastal, central, and far-central regions of the storm—were able to reproduce the wave growth and decay processes with higher accuracy than forecast data. In contrast, GFS forecast data not only underestimated wave amplitudes but also exhibited significant deviations in peak timing and spectral structure.

5. Conclusions

In this study, using two different data sources—GFS forecast data and GFS reanalysis data—the performance of atmospheric and wave models in reconstructing the conditions of Tropical Storm Asna was evaluated. The results showed that, due to the limited availability of high-quality forecast input data, the numerical forecasts produced at the regional level deviated significantly from reality. Specifically, the atmospheric model forced with GFS forecast input failed to accurately represent the intensity and structure of surface winds, and this weakness was directly reflected in the WW3 wave model. As a result, the significant wave height at different stations was lower than the observed values or the ERA5 reanalysis simulations, and the timing of the wave peaks was accompanied by unrealistic delays and fluctuations.

In contrast, the GFS reanalysis data successfully reproduced the wave growth and decay processes, as well as the temporal and spatial structure of the storm, with higher accuracy. However, due to their retrospective nature, these data cannot be used for operational forecasting and, in practice, are not applicable for real-time prediction of ocean–atmosphere conditions.

These results clearly demonstrate that the lack of high-quality and up-to-date atmospheric input data is the main obstacle to producing accurate atmosphere–ocean forecasts in the target regions. In situations where global operational datasets such as forecast or reanalysis GFS alone are unable to fully represent the dynamic and thermodynamic characteristics of tropical cyclones in the northern Indian Ocean, sole reliance on these data leads to significant errors in forecasting wind intensity, wave height, and event timing.

Accordingly, the necessity of developing and deploying a localized atmosphere–ocean model at both global and regional scales is becoming increasingly evident. Such a model, by incorporating local observational data (satellite, buoy, and coastal stations) and advanced data fusion methods, can provide more accurate initial and boundary conditions and, as a result, generate numerical forecasts with higher accuracy and reliability. Achieving this goal will strengthen scientific and operational capabilities in the field of physical oceanography and enable the application of modeling results in secondary marine and coastal activities such as storm crisis management, maritime safety, coastal structure design, and the sustainable exploitation of marine resources across coastal and offshore areas.

8. References

[1] Aboobacker, V. M., Vethamony, P., & Rashmi, R. (2011). "Shamal" swells in the Arabian Sea and their influence along the west coast of India. Journal of Geophysical Research: Oceans, 116(C11).

[2] Alaka, G. J., et al. (2020). A Hydrodynamical Atmosphere–Ocean Coupled Modeling System for Multiple Tropical Cyclones. Atmosphere, 11(8), 869.

[3] Behera, M. R., Bhaskaran, P. K., & Venkatesan, R. (2013). Wave hindcast experiments in the Indian Ocean using WAVEWATCH III: Validation and applications. Natural Hazards, 69(1), 509–532.

[4] Carnegie Endowment for International Peace. (2023). The Indian Ocean Strategic Map.

[5] Camargo, S. J., & Sobel, A. H. (2005). Western North Pacific tropical cyclone intensity and ENSO. Journal of Climate, 18(15), 2996–3006.

[6] Chen, S. S., Zhao, W., Donelan, M. A., & Tolman, H. L. (2013). Coupled atmosphere–wave–ocean models for improving hurricane intensity prediction. Monthly Weather Review, 141(11), 3999–4014.

[7] Davis, A. E., & Balls, J. N. (2022). The Indian Ocean Region

in the 21st Century: Geopolitical, Economic, and Environmental Ties. Australia India Institute, University of Melbourne.

[8] Emanuel, K. (2003). Tropical cyclones. Annual Review of Earth and Planetary Sciences, 31(1), 75–104.

[9] Fan, Y., Ginis, I., & Hara, T. (2009). The effect of wind–wave–current interaction on air–sea momentum fluxes and ocean response in tropical cyclones. Journal of Physical Oceanography, 39(4), 1019–1034.

[10] GDACS (2024). Tropical Cyclone ASNA-24 Report. Global Disaster Alert and Coordination System.

[11] Gray, W. M. (1968). Global view of the origin of tropical disturbances and storms. Monthly Weather Review, 96(10), 669–700.

[12] Holthuijsen, L. H. (2007). Waves in Oceanic and Coastal Waters. Cambridge University Press.

[13] Irfan, S. (2021). Geopolitical and Geostrategic Importance of the Indian Ocean: Challenges and Vulnerabilities for Regional Powers. Jahan-e-Tahqeeq Journal.

[14] Liu, Q., Rogers, W. E., Babanin, A. V., Young, I. R., Romero, L., Zieger, S., Qiao, F., & Guan, C. (2019). Observation-based source terms in the third-generation wave model WAVEWATCH III: Updates and verification. Journal of Physical Oceanography, 49(2), 489–517

[15] Kikuchi, K., Wang, B., & Kajikawa, Y. (2012). BSISO: Intraseasonal variability of the Asian summer monsoon. Climate Dynamics, 39(5), 1065–1082.

[16] Komaromi, W. A., Reinecke, P. A., Doyle, J. D., & Moskaitis, J. R. (2021). The Naval Research Laboratory's Coupled Ocean–Atmosphere Mesoscale Prediction System-Tropical Cyclone Ensemble (COAMPS-TC Ensemble). Weather and Forecasting, 36(2), 499–517.

[17] Komen, G. J., Cavaleri, L., Donelan, M., Hasselmann, K., Hasselmann, S., & Janssen, P. A. E. M. (1994). Dynamics and Modelling of Ocean Waves. Cambridge University Press.

[18] Knutson, T. R., et al. (2020). Tropical cyclones and climate change assessment: Part I. Detection and attribution. Bulletin of the American Meteorological Society, 101(3), E303–E322.

[19] Raj, A., Kumar, B. P., Remya, P. G., Sreejith, M., & Nair, T. M. B. (2023). Assessment of the forecasting potential of WAVEWATCH III model under different Indian Ocean wave conditions. Journal of Earth System Science, 132(32).

[20] Ramsay, H. (2017). Global Climatology of Tropical Cyclones. Oxford Research Encyclopedia of Natural Hazard Science.

[21] Remya, P. G., Kumar, R., & Basu, S. (2012). Evaluation of source term packages in WAVEWATCH III for the Arabian Sea. Ocean Modelling, 47, 55–73.

[22] The WAMDI Group. (1988). The WAM model—A third generation ocean wave prediction model. Journal of Physical Oceanography, 18(12), 1775–1810.

[23] Tolman, H. L. (2009). User manual and system documentation of WAVEWATCH III version 3.14. NOAA/NWS/NCEP/MMAB Technical Note.

[24] Warner, J. C., Armstrong, B., He, R., & Zambon, J. B. (2010). Development of a Coupled Ocean– Atmosphere–Wave–Sediment Transport (COAWST) Modeling System. Ocean Modelling, 35(3), 230–244.

[25] World Meteorological Organization (WMO). (2024). Tropical Cyclone Climatology. Fact Sheet.

[26] www.gebco.net/